Journal of Applied Polymer Science

Synthesis and Properties of Fluorescent Light-Emitting Polyamide Hybrids with Reactive Nanosilica by Epoxide Functionalization

Raouf Alizadeh, Mousa Ghaemy, Maasoomeh Bazzar, Farzaneh Hashemi Nasr
Polymer Research Laboratory, Faculty of Chemistry, Mazandaran University, Babolsar, Iran
Correspondence to: M. Ghaemy (E-mail: ghaemy@umz.ac.ir)

ABSTRACT: A series of poly(carbazole-quinoxaline-amide)s (PCQAs) containing phenyl and long alkyl chain as pendants was synthesized from polycondensation between a new diamine with a synthesized and several commercial dicarboxylic acids using Yamazaki's method. PCQAs had inherent viscosities and weight average molecular weights ($\overline{M}_w$) in the range of 0.48–0.62 dL g^{-1} and 51,600–58,500 g mol^{-1}, respectively. These luminescent polymers are readily soluble in a variety of organic solvents and formed low-colored and tough thin films. In this study, silane modified SiO_2 ($mSiO_2$) nanoparticles were prepared, characterized and used with PCQAs in preparation of nanocomposites via solution blending method. The interfacial interaction strength between $mSiO_2$ and the polymer–matrix enhanced thermal stability ($T_{10\%}$, from 463°C to 500°C) and mechanical strength (from 100 MPa to 150 MPa) for composite containing 30 wt % $mSiO_2$ in comparison with the pure polyamide. These materials showed good ability for extraction–elimination of metal ions such as Cr^{6+}, Cr^{3+}, Co^{2+}, Zn^{2+}, Pb^{2+}, Cd^{2+}, and Hg^{2+} from aqueous solutions either individually or in the mixture at various pH. © 2013 Wiley Periodicals, Inc. J. Appl. Polym. Sci. **2014**, *131*, 40219.

KEYWORDS: composites; mechanical properties; nanoparticles; nanowires and nanocrystals; polyamides; thermal properties

Received 22 July 2013; accepted 20 November 2013
DOI: 10.1002/app.40219

INTRODUCTION

Numerous attempts have been made to improve the processing properties of polyamides, particularly, by improving their solubility and fusibility, while maintaining good thermal stability. The incorporation of flexible linkages,[1,2] flexible side chains,[3] distortion of molecular symmetry by meta-catenated aromatic units,[4–6] introduction of bulky pendant into the polymer chain[7–11] and forming a noncoplanar structure[12–14] will create amorphous polymers with characteristic features which can be considered as high performance materials in advanced technologies. Generally, the incorporation of aromatic heterocyclic rings such as quinoxaline into the macromolecular chain remarkably improves the thermal stability of polymers[15,16] and also due to high electron affinity it has been successfully incorporated into polymers to apply as the electron-transport and electroluminescent materials.[17–19] Carbazole and its many derivatives can be functionalized and thus have been covalently incorporated into polymeric systems, both in main chain as building blocks and in side chains as pendent groups.[20–22]

Polymer/silica nanocomposites have attracted substantial academic interest and many works have studied the structure, properties and possible applications of different polymer–silica hybrids, using poly(caprolactone), polyimide and polyamide.[23–26] The chemical grafting of preformed functionalized polymers on to the solid nanosized substrate is a useful strategy for preparation of polymer nanocomposites.[27]

In the present work, synthesis of a new diamine and diacid is reported having quinoxaline and long-chain substituted carbazole in their structures. The monomers were characterized by spectral and elemental analyses, and used in preparation of poly (carbazole-quinoxaline-amide) (PCQA) by direct phosphorylation polycondensation of Yamazaki method.[28] The polyamides were characterized by spectral and elemental analyses, viscosity measurement and X-ray diffraction (XRD) methods, and used in preparation of chemically bonded nanocomposites with $mSiO_2$ nanoparticles. The properties of polyamides and the nanocomposites such as thermal, solubility and photophysical were investigated to establish a structure–property relationship, and also their ability to remove environmentally toxic heavy metal ions such as Cr^{6+}, Cr^{3+}, Co^{2+}, Zn^{2+}, Pb^{2+}, Cd^{2+}, and Hg^{2+} from aqueous media have been studied.

EXPERIMENTAL

Materials

All materials and solvents were purchased either from Merck or Fluka (Germany). γ-glycidoxypropyltriethoxysilane (GPTES), SiO_2 (with grain diameter of 10 nm, a density of 4 g cm^{-3} and specific surface area of 15 m^2 g^{-1}), hydrazine monohydrate, Pd/C,

triphenyl phosphite (TPP), and solvents such as glacial acetic acid, ethanol, and methanol were used as received. *N*,*N*-Dimethylformamide (DMF), *N*-methyl-2-pyrrolidinone (NMP), *N*,*N*-dimethylacetamide (DMAc), dimethyl sulfoxide (DMSO), and pyridine were purified by distillation over calcium hydride under reduced pressure and stored over 4 Å molecular sieves. Tetrahydrofuran was dried by sodium before use. Different reagent-grade commercial dicarboxylic acids such as terephthalic acid, isophthalic acid, 2,6-pyridinedicarboxylic acid, 2,2′-bis(4-carboxyphenyl)hexafluoropropane, adipic acid, and sebacic acid were used after drying in the vacuum oven. LiCl and $CaCl_2$ were dried at 180°C in a vacuum oven for 14 h.

Monomer Synthesis

Compounds 9-octyl-9H-carbazole (OC), 1,1′-(9-octyl-9H-carbazole-3,6-diyl)bis(2-phenylethanone) (DO), and 2,2′-(9-octyl-9H-carbazole-3,6-diyl)bis(1-phenylethane-1,2-dione) (BDO) were synthesized following a method reported in our previous work.[29]

Compound (OC). Yield = 85%, and proton nuclear magnetic resonance (^{1}H NMR; $CDCl_3$): $\delta = 0.79$ (t, 3H, CH, $J = 7.6$ Hz), 1.17–1.22 (m, 10H, CH), 1.76–1.80 (m, 2H, CH), 4.51 (t, 2H, CH, $J = 7.2$ Hz), 7.21–7.39 (m, 2H, Ar–H), 7.46–7.62 (m, 4H, Ar–H), 8.20 (d, 2H, Ar–H, $J = 7.9$ Hz). Elemental analysis calculated for $C_{20}H_{25}N$ (279.42 g mol^{-1}): C, 85.97%; H, 9.02%; N, 5.01%. Found: C, 85.88%; H, 9.14%; N, 4.98%.

Compound (DO). Yield = 83%, and ^{1}H NMR (DMSO-d_6): $\delta = 0.96$ (t, 3H, CH, $J = 7.2$ Hz), 1.14–1.22 (m, 10H, CH), 1.73–1.80 (m, 2H, CH), 3.57 (s, 4H, CH), 4.53 (t, 2H, CH, $J = 7.0$ Hz), 7.25–7.27 (m, 4H, Ar–H), 7.29–7.38 (m, 6H, Ar–H), 7.75 (d, 2H, Ar–H, $J = 8.4$ Hz), 8.18 (d, 2H, Ar–H, $J = 2.0$ Hz), 9.22 (d, 2H, Ar–H, $J = 1.6$ Hz). Carbon nuclear magnetic resonance (^{13}C NMR; 100 MHz, DMSO-d_6, δ in ppm): 14.35, 22.44, 26.77, 28.92, 29.00, 29.10, 31.57, 43.24, 45.01, 110.45, 122.78, 126.54, 126.86, 129.02, 129.13, 129.91, 130.16, 135.47, 136.20, 197.32. Elemental analysis calculated for $C_{36}H_{37}NO_2$ (515.68 g mol^{-1}): C, 83.85%; H, 7.23%; N, 2.72%. Found: C, 83.72%; H, 7.34%; N, 2.81%.

Compound (BDO). Yield = 70%, m.p. = 128–131°C and ^{1}H NMR (DMSO-d_6): $\delta = 0.77$ (t, 3H, CH, $J = 7.2$ Hz), 1.13–1.23 (m, 10H, CH), 1.76–1.80 (m, 2H, CH), 4.52 (t, 2H, CH, $J = 7.2$ Hz), 7.62 (t, 4H, Ar–H, $J = 7.2$ Hz), 7.75–7.80 (m, 2H, Ar–H), 7.90–7.96 (m, 6H, Ar–H), 8.10 (dd, 2H, Ar–H, $J = 1.6$ Hz), 9.05 (d, 2H, Ar–H, $J = 1.6$ Hz). ^{13}C NMR (DMSO-d_6): $\delta = 14.35$, 22.44, 26.77, 28.92, 29.00, 29.10, 31.57, 45.01, 111.75, 123.84, 124.18, 129.66, 129.94, 131.19, 132.62, 133.82, 136.07, 137.60, 195.98, 196.01. Elemental analysis calculated for $C_{36}H_{33}NO_4$ (543.65 g mol^{-1}): C, 79.53%; H, 6.12%; N, 2.58%. Found: C, 79.39%; H, 6.23%; N, 2.50%.

Synthesis of 3,6-Bis(7-nitro-3-phenylquinoxaline-2-yl)-9-octyl-9H-carbazole. In a 100 mL round-bottomed two-necked flask equipped with a condenser and magnetic stirrer bar and a nitrogen gas inlet tube, a mixture of 2.81g (18.4 mmol) 4-nitro-o-phenylenediamine, 5 g (9.2 mmol) BDO and 50 mL glacial acetic acid was refluxed for 24 h. After cooling to room temperature, it was poured into 200 mL cold water. The orange precipitates was filtered, washed with water, and dried. The yield of the crude product was 6.47 g (90%) with the melting point of 176°C. Fourier transform infrared spectroscopy (FT-IR; KBr): 3030 (aromatic C—H), 2925 (aliphatic C—H), 1598 (C═N), 1524, 1342 cm^{-1} (NO_2); ^{1}H NMR (DMSO-d_6): $\delta = 0.76$ (t, 3H, CH, $J = 6.8$ Hz), 1.11–1.15 (m, 10H, CH), 1.61 (b, 2H, CH), 4.20 (b, 2H, CH), 7.24–7.48 (m, 14H, Ar–H), 8.16–8.22 (m, 4H, Ar–H), 8.39–8.44 (m, 2H, Ar–H), 8.73–8.76 (m, 2H, Ar–H). ^{13}C NMR (DMSO-d_6): $\delta = 14.23$, 22.84, 26.81, 28.89, 29.07, 29.24, 31.57, 42.92, 109.36, 122.51, 123.33, 123.78, 124.92, 125.15, 128.56, 129.90, 130.78, 124.92, 125.15, 128.56, 129.90, 130.78, 139.67, 141.36, 142.99, 143.53, 147.43, 147.81, 155.76, 156.29. Elemental analysis calculated for $C_{48}H_{39}N_7O_4$ (777.87 g mol^{-1}): C, 74.11%; H, 5.05%; N, 12.60%. Found: C, 74.02%; H, 5.26%; N, 12.41%.

Synthesis of 3,3′-(9-Octyl-9H-carbazole-3,6-diyl)bis(2-phenylquinoxaline-6-amine). Into a 250-mL three-necked flask equipped with a dropping funnel and a reflux condenser, 3.88 g (5 mmol) 3,6-bis(7-nitro-3-phenylquinoxaline-2-yl)-9-octyl-9H-carbazole (DNQC), 0.2 g palladium on activated carbon (Pd/C, 10%), and 100 mL ethanol were added, and after heating to refluxing temperature with stirring, 5 mL hydrazine monohydrate was added dropwise for 1 h. After the addition of hydrazine monohydrate, the mixture was refluxed for an additional 5 h and the product precipitated during this period. The mixture was then added to enough ethanol to dissolve 3,3′-(9-octyl-9H-carbazole-3,6-diyl)bis(2-phenylquinoxaline-6-amine) (DAQC) and filtered to remove Pd/C. After cooling, the precipitated crystals were isolated by filtration and dried in vacuum at 80°C. The yield of the reaction was 86% (3.11 g) and the melting point was 173°C. FT-IR (KBr): 3405, 3345 (N–H); 3028 (aromatic C—H); 2925 (aliphatic C—H); 1627 cm^{-1} (C═N). ^{1}H NMR (DMSO-d_6): $\delta = 0.80$ (t, 3H, CH, $J = 6.8$ Hz), 1.19 (m, 10H, CH), 1.71 (b, 2H, CH), 4.35 (b, 2H, CH), 6.10 (s, 4H, N–H), 7.01 (m, 2H, Ar–H), 7.24–7.50 (m,16H, Ar–H), 7.96–7.85 (m, 2H, Ar–H), 8.16–8.20 (dd, 2H, Ar–H, $J = 11.2$ Hz). ^{13}C NMR (DMSO-d6): $\delta = 14.37$, 22.47, 26.88, 28.99, 29.08, 29.14, 31.59, 42.86, 105.12, 105.21, 122.38, 128.35, 128.66, 129.94, 130.90, 134.87, 135.30, 140.43, 140.78, 143.22, 143.64, 147.82, 148.30, 150.97, 151.23, 152.91. Elemental analysis calculated for $C_{48}H_{43}N_7$ (717.90 g mol^{-1}): C, 80.31%; H, 6.04%; N, 13.66%. Found: C, 80.11%; H, 5.88%; N, 13.47%.

Synthesis of 3,3′-(9-Octyl-9H-carbazole-3,6-diyl)bis(2-phenylquinoxaline-6-carboxylic acid). This compound was synthesized similar to the procedure used for the preparation of DAQC and 3,4-diaminobenzoic acid was used instead of 4-nitro-o-phenylenediamine. The yield of the reaction was 93% (6.65 g) and the melting point was 215°C. FT-IR (KBr): 3500–3100 (OH); 2930 (aliphatic C—H); 1683 (C═O); 1604 cm^{-1} (C═N). ^{1}H NMR (DMSO-d_6): $\delta = 0.79$ (t, 3H, CH, $J = 6.8$ Hz), 1.20 (m, 10H, CH), 1.74 (b, 2H, CH), 4.39 (t, 2H, CH, $J = 6.4$ Hz), 7.34–7.58 (m,14H, Ar–H), 8.22–8.37 (m, 6H, Ar–H), 8.66–8.69 (m, 2H, Ar–H), 13.44 (s, 2H, COOH). Elemental analysis calculated for $C_{50}H_{41}N_5O_4$ (775.89 g mol^{-1}): C, 77.40%; H, 5.33%; N, 9.03%. Found: C, 77.06%; H, 5.18%; N, 9.26%.

Polymer Synthesis

The synthesis of PCQA1 is given as an example to illustrate the general synthetic procedure used to prepare the polyamides.

A mixture of 0.33 g (2 mmol) terephthalic acid (3a), 1.43g (2 mmol) diamine DAQC, 0.6 g calcium chloride, 2.4 mL TPP, 2 mL pyridine, and 10 mL NMP was heated with stirring at 120°C for 12 h. After cooling, the reaction mixture was poured into a large amount of methanol with constant stirring, producing a stringy precipitate that was washed thoroughly with methanol and hot water, collected by filtration, extracted with methanol in a Soxhlet apparatus for 6 h and then dried at 100°C in vacuum for 24 h. The inherent viscosity of the polymer in NMP was measured at a concentration of 0.5 g dL^{-1} at 25°C.

Poly(carbazole-quinoxaline-amide) 1. This polymer was synthesized from DAQC and terephthalic acid. Yield 92% and $\eta_{inh} = 0.62$ dL g^{-1}. FT-IR (KBr): 3325 (N–H); 3060 (aromatic C—H); 2920 (aliphatic C—H); 1672 (C═O); 1620 cm^{-1} (C═N). ^{1}H NMR (DMSO-d_6): $\delta = 0.80$ (b, 3H, CH), 1.18–1.23 (m, 10H, CH), 1.74 (s, 2H, CH), 4.38 (s, 2H, CH), 7.37–7.54 (m, 12H, Ar–H), 8.07–8.31 (m, 12H, Ar–H), 8.81 (s, 2H, Ar–H), 10.97 (s, 2H, N–H amide). Elemental analysis calculated for $C_{56}H_{45}N_7O_2$: C, 79.32%; H, 5.35%; N, 11.56%. Found: C, 79.04%; H, 5.69%; N, 11.28%.

Poly(carbazole-quinoxaline-amide) 2. This polymer was synthesized from DAQC and isophthalic acid. Yield 90% and $\eta_{inh} = 0.56$ dL g^{-1}. FT-IR (KBr): 3336 (N–H); 3060 (aromatic C—H); 2925 (aliphatic C—H); 1679 (C—O); 1622 cm^{-1} (C—N). ^{1}H NMR (DMSO-d_6): $\delta = 0.81$ (b, 3H, CH), 1.10–1.14 (m, 10H, CH), 1.78 (m, 2H, CH), 4.36 (b, 2H, CH), 7.16–7.38 (m, 14H, Ar–H), 8.02–8.39 (m, 10H, Ar–H), 8.83 (m, 2H, Ar–H), 10.99 (s, 2H, N–H amide). Elemental analysis calculated for $C_{56}H_{45}N_7O_2$: C, 79.32%; H, 5.35%; N, 11.56%. Found: C, 78.91%; H, 5.12%; N, 11.34%.

Poly(carbazole-quinoxaline-amide) 3. This polymer was synthesized from DAQC and 2,6-pyridinedicarboxylic acid. Yield 87% and $\eta_{inh} = 0.55$ dL g^{-1}. FT-IR (KBr): 3330 (N–H); 3061 (aromatic C—H); 2916 (aliphatic C—H); 1687 (C—O); 1625 cm^{-1} (C—N). ^{1}H NMR (DMSO-d_6): $\delta = 0.81$ (s, 3H, CH), 1.15–1.23 (m, 10H, CH), 1.85 (m, 2H, CH), 4.23 (m, 2H, CH), 7.36–7.54 (m, 15H, Ar–H), 8.31–8.42 (m, 10H, Ar–H), 11.42(s, 2H, N–H amide). Elemental analysis calculated for $C_{55}H_{44}N_8O_2$: C, 77.81%; H, 5.22%; N, 13.20%. Found: C, 77.53%; H, 4.89%; N, 13.51%.

Poly(carbazole-quinoxaline-amide) 4. This polymer was synthesized from DAQC and 2,2′-bis(4-carboxyphenyl) hexafluoropropane. Yield 87% and $\eta_{inh} = 0.50$ dL g^{-1}. FT-IR (KBr): 3338 (N–H); 3066 (aromatic C—H); 2931 (aliphatic C—H); 1685 (C—O); 1626 cm^{-1} (C—N). ^{1}H NMR (DMSO-d_6): $\delta = 0.81$ (b, 3H, CH), 1.17–1.25 (m, 10H, CH), 1.71 (m, 2H, CH), 4.37 (b, 2H, CH), 7.34–7.54 (m,16H, Ar–H), 8.13–8.31 (m, 12H, Ar–H), 8.74 (m, 2H, Ar–H), 10.96 (s, 2H, N–H amide). Elemental analysis calculated for $C_{65}H_{49}F_6N_7O_2$: C, 72.68%; H, 4.60%; N, 9.13%. Found: C, 72.41%; H, 4.46%; N, 9.30%.

Poly(carbazole-quinoxaline-amide) 5. This polymer was synthesized from DAQC and 3,3′-(9-octyl-9H-carbazole-3,6-diyl)-bis(2-phenylquinoxaline-6-carboxylic acid) (CAQA). Yield 91% and $\eta_{inh} = 0.52$ dL g^{-1}. FT-IR (KBr): 3359 (N–H); 3062 (aromatic C—H); 2920 (aliphatic C—H); 1679 (C—O); 1621 cm^{-1} (C—N). ^{1}H NMR (DMSO-d_6): $\delta = 0.80$ (m, 3H, CH), 1.17–1.24 (m, 10H, CH), 1.74 (b, 2H, CH), 4.38 (b, 2H, CH), 7.36–7.55 (m, 16H, Ar–H), 8.21–8.42 (m, 6H, Ar–H), 11.13 (s, 2H, N–H amide). Elemental analysis calculated for $C_{57}H_{48}N_8O_2$ (877.04 g mol^{-1}): C, 78.06%; H, 5.52%; N, 12.78%. Found: C, 77.78%; H, 6.03%; N, 12.64%.

Poly(carbazole-quinoxaline-amide) 6. This polymer was synthesized from DAQC and adipic acid. Yield 85% and $\eta_{inh} = 0.48$ dL g^{-1}. FT-IR (KBr): 3330 (N–H); 3062 (aromatic C—H); 2918 (aliphatic C—H); 1683 (C—O); 1618 cm^{-1} (C—N). ^{1}H NMR (DMSO-d_6): $\delta = 0.78$ (3H, CH), 1.13–1.53 (m, 10H, CH), 1.75 (b, 10H, CH), 4.34 (b, 2H, CH), 7.12 (b, 2H, Ar–H), 7.30–7.47 (m, 14H, Ar–H), 7.90 (m, 2H, Ar–H), 8.04 (b, 2H, Ar–H), 8.06 (b, 2H, Ar–H), 10.46 (s, 2H, N–H amide). Elemental analysis calculated for $C_{54}H_{49}N_7O_2$: C, 78.33%; H, 5.96%; N, 11.84%. Found: C, 78.58%; H, 5.71%; N, 12.04%.

Poly(carbazole-quinoxaline-amide) 7. This polymer was synthesized from DAQC and sebacic acid. Yield 91% and $\eta_{inh} = 0.53$ dL g^{-1}. FT-IR (KBr): 3310 (N–H); 3057 (aromatic C—H); 2927 (aliphatic C—H); 1666 (C—O); 1618 cm^{-1} (C—N). ^{1}H NMR (DMSO-d_6): $\delta = 0.77$ (b, 3H, CH), 1.15–1.32 (m, 12H, CH), 1.65 (b, 4H, CH), 2.08 (s, 2H, CH), 4.30 (b, 2H, CH), 7.08 (s, 2H, Ar–H), 7.29–7.46 (m, 10H, Ar–H), 7.87 (m, 2H, Ar–H), 8.05 (s, 2H, Ar–H), 8.27 (s, 2H, Ar–H), 8.61 (b, 4H, Ar–H), 10.39 (s, 2H, N–H amide). Elemental analysis calculated for $C_{58}H_{57}N_7O_2$: C, 88.35%; H, 6.50%; N, 11.09%. Found: C, 88.59%; H, 6.23%; N, 11.30%.

Surface Modification of SiO_2 Nanoparticles

The coupling agent of GPTES was introduced to ensure good dispersion and improvement in interfacial interaction between SiO_2 nanoparticles and polymer matrix. The surface modification of SiO_2 particles was carried out as follows. A suspension of 1 g SiO_2 particles in 30 mL ethanol and water (50/50, v/v) in a 50 mL round bottomed flask equipped with a reflux condenser, a nitrogen gas inlet tube and a magnetic stir was sonicated 30 min using a 150-W water ultrasonic bath. 1 g GPTES was added to the solution and the mixture was stirred at 80°C for 3 h and then left at room temperature for 24 h. Finally, the particles were separated from solution by filteration and were sonicated twice in methanol (each time for 30 min) to remove unreacted molecules, and then dried in a vacuum oven at 110°C for 24 h. The modified SiO_2 ($mSiO_2$) nanoparticles were kept under vacuum in order to protect the nanoparticles surface from moisture.

Preparation of $mSiO_2$/PCQA Nanocomposites

0.1 g of a polyamide (PCQA) was dissolved in 20 mL dry DMAc. Then a certain amount of modified SiO_2 nanoparticles (15 wt % and 30 wt % based on the weight of PCQA) was added to the resulting solution and the mixture was ultra sonicated for 30 min at 70°C under N_2 and then was continuously stirred at this temperature for 5 h. The homogeneous mixture was loaded in a plane glass vessel placed horizontally in a vacuum oven, gradually was heated to evaporate the solvent and then dried at 70°C for 24 h to obtain polymer/$mSiO_2$ film.

Measurements

Elemental analysis was run in a Flash EA 1112 series analyzer. FT-IR spectra were recorded on a Bruker Tensor 27

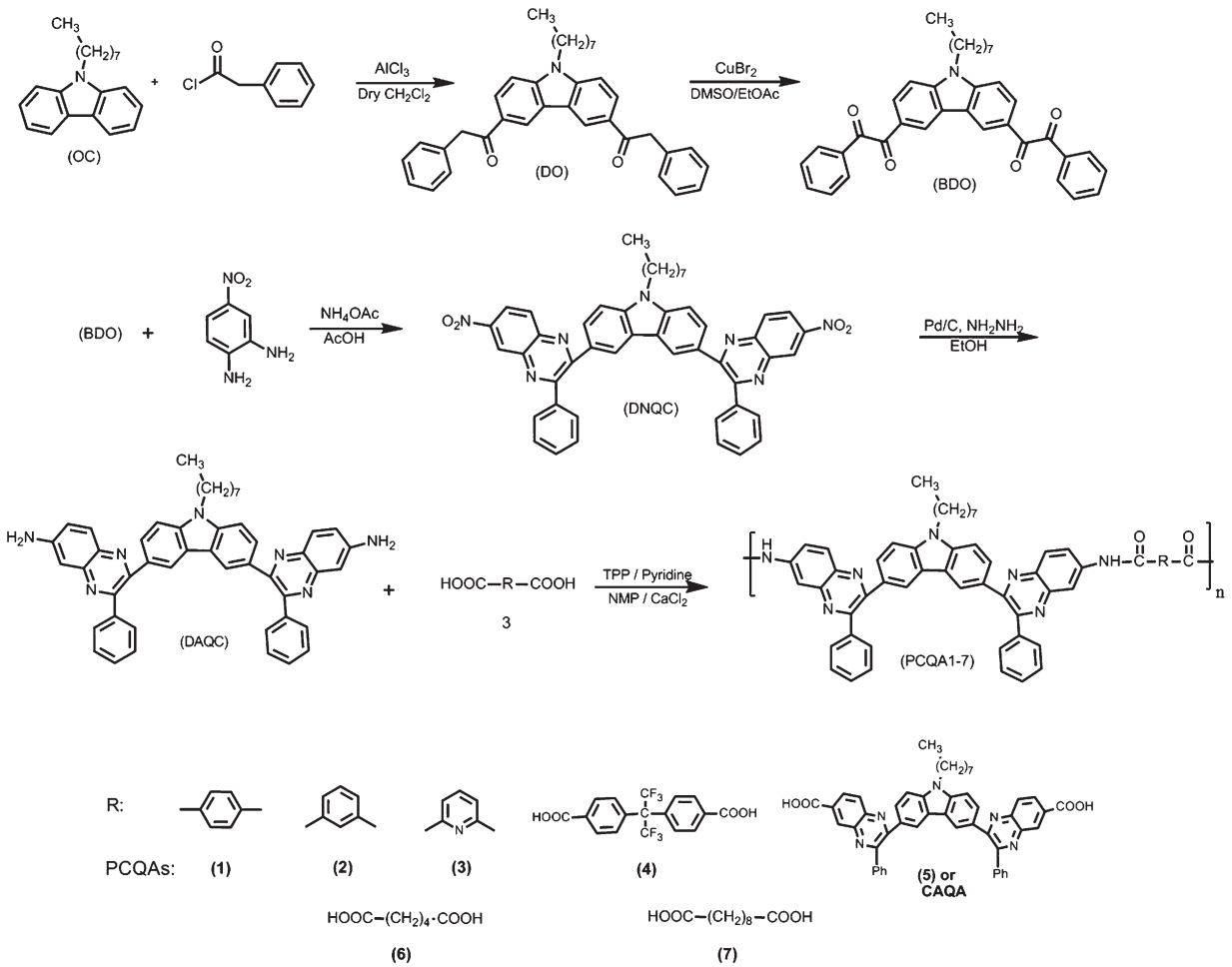

Scheme 1. Synthesis procedure for the preparation of monomers and PCQAs.

spectrometer. The spectra of solids were obtained using KBr pellets. ^{1}H NMR and ^{13}C NMR spectra were recorded on a 400 MHz and 100 MHz Bruker Advance DRX instrument, respectively, using DMSO-d_6 as solvent and tetramethyl silane as an internal standard. The inherent viscosities were measured using an Ubbelohde viscometer with polymer concentration of 0.5 g dL^{-1} in NMP at 25°C. Melting points were determined in open capillaries with IA 9200 Series Digital Melting Point apparatus. Thermogravimetric analysis (TGA) was conducted with a TGA-50 analyzer in the temperature range of 30–700°C at a heating rate of 10°C min^{-1} under nitrogen atmosphere. Differential scanning calorimeter (DSC) analysis was performed on a Perkin-Elmer Pyris 6 calorimeter at a heating rate of 10°C min^{-1} under nitrogen (20 cm^3 min^{-1}). Glass transition temperatures (T_gs) were read at the middle of the transition in the heat capacity of the second heating scan after quick cooling from 350°C to ambient temperature. Dynamic mechanical thermal analysis (DMTA) was carried out on a Polymer Laboratories instrument (Model MK-II, Surrey, UK) over a temperature range of 25–300°C at 1 Hz and a heating rate of 5°C min^{-1}. Relaxation temperatures were determined from corresponding peak top temperatures seen on the damping (tan δ) curves. Ultraviolet (UV)-visible (vis) and fluorescence emission spectra were recorded on a Cecil 5503 and Perkin-Elmer LS-3B spectrophotometers, respectively. The gel permeation chromatography (GPC) measurements were conducted at 30°C with a Perkin-Elmer instrument equipped with a differential refractometer detector. The columns used were packed with a polystyrene/divinylbenzene copolymer (PL gel MIXED-B from Polymer Laboratories) with DMF as fluent at a flow rate of 1 mL min^{-1}. Calibration of the instrument was done with monodisperse polystyrene standards. Atomic force microscopy (AFM) Easy

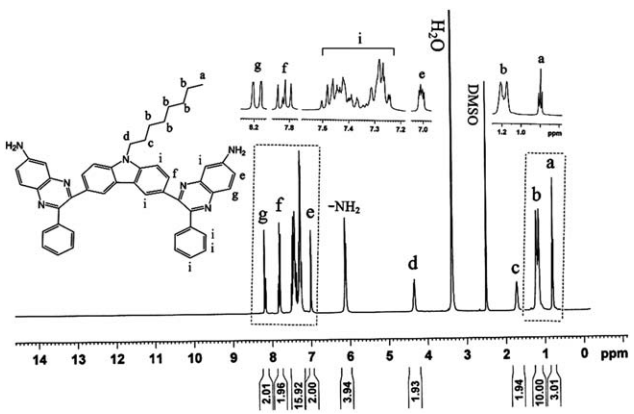

Figure 1. ^{1}H NMR spectrum of DAQC in DMSO-d_6.

Table I. Inherent Viscosity, Average Molecular Weights and Solubility of PCQAs and Nanocomposites

				Solubility [a]							
Polymer Code	η_{inh} (dL/g)[b]	$\overline{M}_n$[c] (g/mol)	$\overline{M}_w$[c] (g/mol)	NMP	DMSO	DMF	DMAc	Py	THF	m-Cresol	CH_3CN
PCQA1	0.62	31000	58500	++	++	++	++	++	±	+	-
PCQA 2	0.56	29800	56500	++	++	++	++	++	±	+	-
PCQA 3	0.55	28600	53000	++	++	++	++	++	±	+	-
PCQA 4	0.50	30500	57500	++	++	++	++	++	+	+	-
PCQA 5	0.52	34000	58300	++	++	++	++	++	+	++	-
PCQA 6	0.48	26300	51600	++	++	++	++	++	+	++	-
PCQA 7	0.53	27500	52800	++	++	++	++	++	+	++	-
PCQA 1/15%SiO_2	-	-	-	±	±	±	±	-	-	-	-
PCQA 5/15%SiO_2	-	-	-	±	±	±	±	-	-	-	-
PCQA 7/15%SiO_2	-	-	-	±	±	±	±	-	-	-	-
PCQA 1/30%SiO_2	-	-	-	-	-	-	-	-	-	-	-
PCQA 5/30%SiO_2	-	-	-	-	-	-	-	-	-	-	-
PCQA 7/30%SiO_2	-	-	-	-	-	-	-	-	-	-	-

Abbreviations: NMP, N-methyl pyrrolidone; DMSO, dimethyl sulfoxide; DMF, N,N-dimethyl formamide; DMAc, N,N-dimethyl acetamide; Py, pyridine; THF, tetrahydrofuran.
[a] Solubility: ++, soluble at room temperature; +, soluble on heating at 60 °C; ±, partially soluble on heating at 60 °C; -, insoluble on heating at 60 °C.
[b] Measured at a polymer concentration of 0.5 g/dL in NMP at 30 °C.
[c] Average molecular weights relative to polystyrene standard in DMF by GPC.

Scan 2 Flex AFM (Swiss Co) was used to investigate the surface phase and topography of the pure polyamides and nanocomposites. XRD patterns were recorded by X-ray diffractometer (GBC MMA Instrument) with Be filtered Cu Ka radiation (1.5418 Å) operating at 35.4 kV and 28 mA. The scanning range of 2θ was set between 5° and 80° with scan rate of 0.058 s^{-1}. Branson S3200 (50 kHz, 150 W) ultrasonic bath was used for better dispersion of nanoparticles. The mechanical properties of polymer films was measured at room temperature on an universal testing machine (SANTAM, model STM-20, IRAN) with a 5 KN load cell using film strips of 11 mm width 30 mm length and 1 mm thickness. The gauge length was 30 mm and the crosshead speed was 5 mm min^{-1}. An average of at least five individual measurements was used for each sample. For preparation of polymer film, a solution was made by dissolving about 0.5 g of a polyamide sample in 10 mL of DMF. The homogeneous solution was poured into a 9-cm glass Petri dish and placed in an oven (70°C) overnight to evaporate the solvent. The semi-dried film was further dried in vacuum at 130°C for 5 h. Water absorption measurements were determined gravimetrically at room temperature using two test methods. Method I: Immersion of a polymer film (3 mm ×3 mm) in water at 25°C for 24 h, followed immediately by weighing. Method II: Boiling a polymer film in water at 100°C for 30 min, and its weight difference before and after immersion was determined. The solid–liquid extraction of Cr^{3+}, Co^{2+}, Pb^{2+}, Cd^{2+} as their chloride salts, Hg^{2+} as nitrate salts, and Cr^{6+} as ($K_2Cr_2O_7$) was carried out either individually or in the mixture at different pH values. Approximately 50 mg of the appropriate polymer powder was shaken with 50 mL of an aqueous solution of the metal salt (at pH = 7–8) for a week at 25°C (equilibrium was assessed in less than 3 days). The initial concentration of salts was 20 mg L^{-1}. After filtration, the concentration of each metal cation in the liquid phase was determined by atomic absorption (BRAICWFX-130 AA), and direct information regarding the extraction percentage of metal ions by the polymer was obtained using a calibration curve which was made for each metal ion from the standard solutions of 5 ppm, 10 ppm, and 20 ppm.

RESULTS AND DISCUSSION

Synthesis and Characterization of PCQAs and Nanocomposites

The main purpose of this work was to investigate the effect of two important functional groups namely carbazol and quinoxaline rings in the main chain of polyamides on the properties

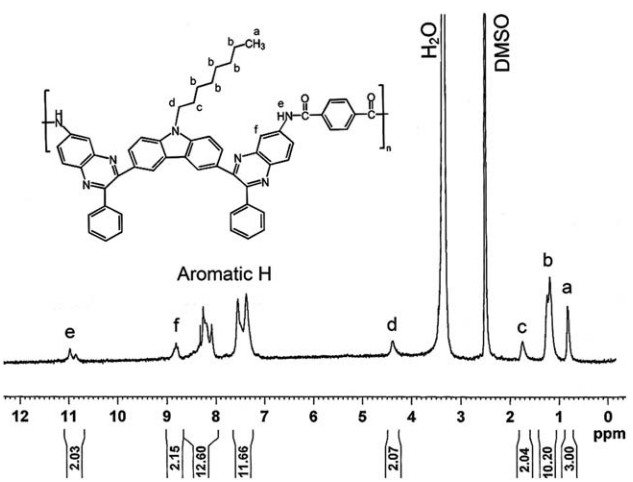

Figure 2. [1] H NMR spectrum of PCQA1 in DMSO-d_6.

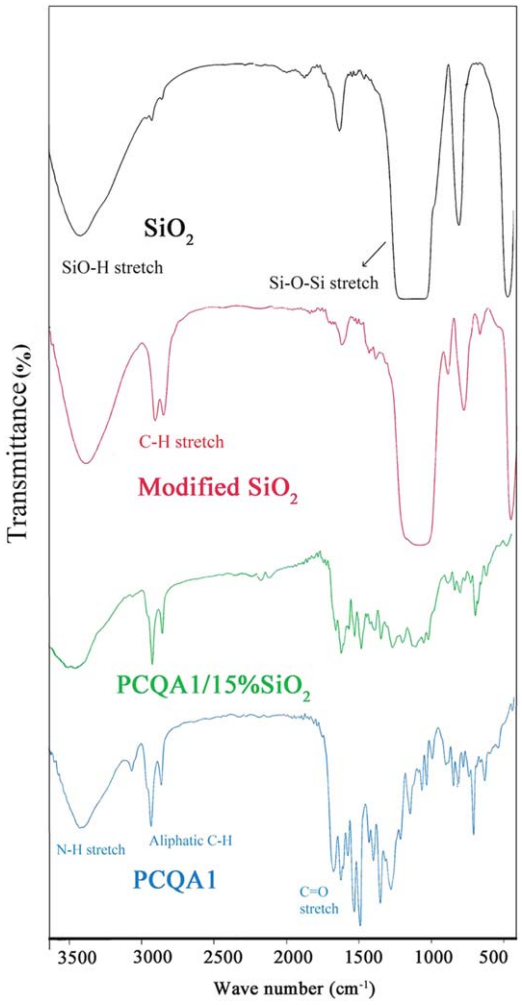

such as solubility, thermal, strength and photophysical. Thus, a new diamine was synthesized through multisteps procedure (Scheme 1). First, the 9H-carbazole was allowed to react with 1-bromooctane to prepare its OC derivative.[29] This reagent is further involved in a Friedel–Crafts reaction with 2-phenylacetyl chloride to give compound (DO) in high yield. The oxidation of the resulting bisbenzyl compound is then accomplished in the presence of cupric bromide and DMSO in ethyl acetate to afford a new bis(α-diketone) (BDO) with a 75% overall yield. The reaction of bis(α-diketone) with 4-nitro-o-phenylenediamine was carried out to obtain DNQC. Finally, reduction of nitro groups of DNQC via hydrazine monohydrate and Pd/C afforded the desired diamine DAQC. Elemental analysis, FT-IR, ^{1}H NMR and ^{13}C NMR spectroscopies were used to identify the structures of the synthesized compounds. According to the FT-IR spectera of DNQC and DAQC absorption bands representative of the nitro group were identified by the asymmetrical and symmetrical stretchings at 1524 cm^{-1} and 1342 cm^{-1}, respectively. After reduction, the bands for the nitro groups were disappeared and the primary amine absorptions were identified at 3405 cm^{-1} and 3345 cm^{-1}. The band of the C═N stretching was also apparent around 1610 cm^{-1} in both FT-IR spectera of DNQC and DAQC. The ^{1}H NMR specterum of DNQC showed that aromatic protons at the ortho porotion to the nitro group have the largest chemical shift (8.76 ppm) due to the inductive and anisotropic deshielding effect of the nitro group. The ^{1}H and ^{13}C NMR spectra of DAQC show the assignments of the aberved resonances. The primary amine protons appeared at 6.10 ppm and the aliphatic protons of alky side chain appeared in the region 0.80–4.35 ppm (Figure 1).

The protons near the nitrogen atom of carbazol resonate at the highest field than others alky chain protones. Aromatic protons at 7.1–8.2 ppm showed the expected multiplicity and integration

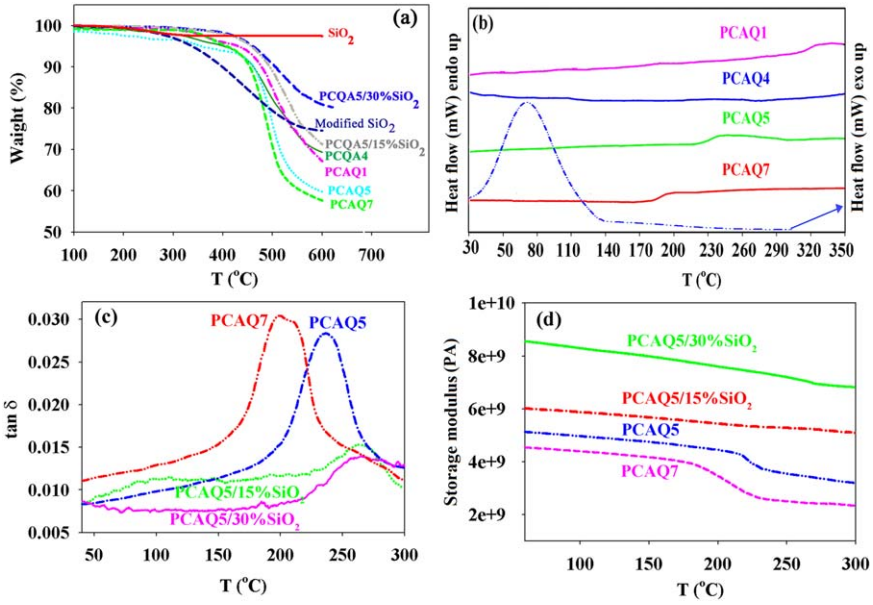

Figure 4. (a) TGA curves of SiO_2, $mSiO_2$, PCQAs and nanocomposites. (b) DSC curves of PCQAs and exothermic peak of cure reaction between $mSiO_2$ and PCQA. (c and d) Tan δ curves and storage modulus of PCQA5 and PCQA7 and nanocomposites, respectively. [Color figure can be viewed in the online issue, which is available at wileyonlinelibrary.com.]

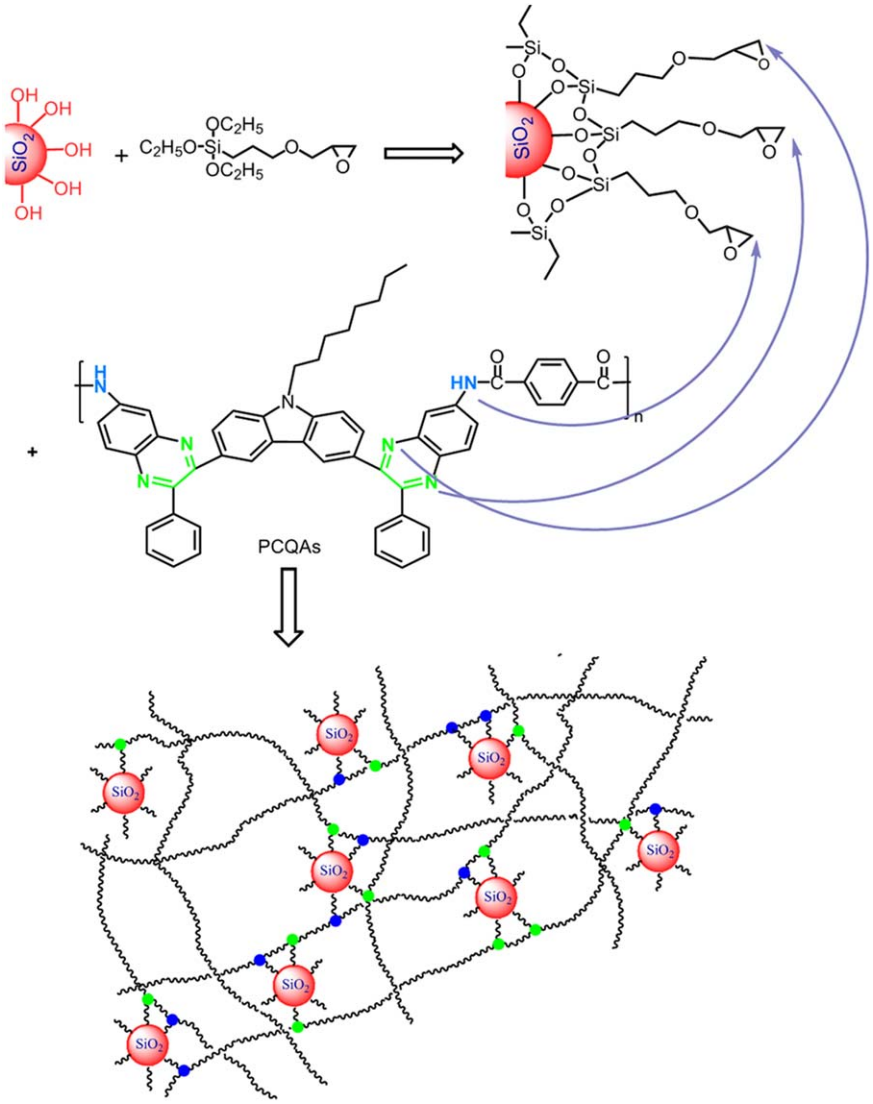

Scheme 2. Reaction scheme for the preparation of nanocomposites. [Color figure can be viewed in the online issue, which is available at wileyonlinelibrary.com.]

values. The ^{13}C NMR spectrum of DAQC monomer showed 18 signals in the regions of 14.3–42.8 ppm related to aromatic carbon and 8 signals corresponding to aliphatic carbon in the region of 105.2–152.9 ppm. Also the FT-IR spectrum of CAQA showed a wide absorption band at 3300 cm^{-1} and a sharp peak at 1680 cm^{-1} characteristic for the carboxylic acid group, and another peak at 1600 cm^{-1} due to C═N in the quinoxaline ring. The structure of CAQA was also identified with ^1H NMR spectrum, as listed in the experimental section, and the peak at 13.44 ppm corresponds to carboxylic O–H resonance. As shown in Scheme 1, PCQAs were synthesized from DAQC with various commercial dicarboxylic acids and with the new dicarboxylic acid (CAQA) by the Yamazaki polycondensation conditions.[28]

All polyamidations proceeded in homogeneous and viscous solutions throughout the reaction and the PCQAs were obtained in almost quantitative yields. The inherent viscosity, the number average molecular weight ($\overline{M}_n$) and the weight average molecular weight ($\overline{M}_w$) of all PCQAs are summarized in Table I. The inherent viscosities of these polymers are in the range of 0.48–0.62 dL g^{-1}. GPC analysis revealed the number average molecular weights ($\overline{M}_n$) and $\overline{M}_w$ of these polymers in the range of 26,300–34,000 g mol^{-1} and 51,600–58,500 g mol^{-1}, respectively. The formation of PCQA was confirmed by elemental analysis, FT-IR and ^1H NMR spectroscopy. All PCQAs showed characteristic absorption bands of the amide group around 3200 (N–H stretching), 1660 (amide carbonyl) and 1620 cm^{-1} (C═N stretching). ^1H NMR spectra confirmed the chemical structure of PCQAs with the amide proton chemical shift observed at about 11 ppm. Disappearance of peak at about 6.10 ppm indicates complete conversion of the amine groups into amides. Figure 2 shows the representative ^1H NMR spectrum of PCQA1 which confirms the proposed structure.

FT-IR spectra of native SiO_2, modified SiO2 and nanocomposite are shown in Figure 3. The spectrum of native SiO_2 only presents

a few absorption peaks; the broad band at 1100 cm^{-1} can be assigned to the characteristic vibration peaks of Si–O groups, and the characteristic stretching vibration peak of hydroxyl group (—OH) on the surface of SiO_2 nanoparticles can be observed at 3447 cm^{-1}. The characteristic peaks of C—H bending of organic methylene at 1385 cm^{-1} and of stretching vibrations at 2920 cm^{-1} and 2851 cm^{-1} appeared after modification of SiO_2 nanoparticles with GPTES. In addition, characteristic absorption peak at 1050–1090 cm^{-1} broadens, this phenomenon reveals that a new absorption peak of Si–O–Si has formed in this range, which is due to the contribution of interaction between siloxane and SiO_2. The above interpretations are enough to manifest that GPTES is bound on the surface of SiO_2 nanoparticles.

Comparison of TGA curves of native SiO_2 and $mSiO_2$ nanoparticles in N_2 [Figure 4(a)] indicates that the weight loss of native SiO_2 is 0.5% in the range of 0–400°C (almost no weight loss over 400°C), which is due to the loss of absorbed moisture. The weight of $mSiO_2$ decreases quickly over 300°C and the loss is about 25% over 550°C, which can be attributed to the thermal decomposition of (GPTES) at high temperature. It can be deduced that the maximum mass fraction of (GPTES) on the surface of SiO_2 is about 25%. Also, previous studies on the adduct formation between 1-substituted imidazole[30,31] and triazole[27,32] with the epoxide group suggested that reaction between more basic pyridine-type nitrogen with the epoxide group leads to a zwitter ionic structure, as shown in Scheme 2.

After doping $mSiO_2$ in PCQAs, intensity of the peaks at 1450–1570 cm^{-1} changes which may be due to protonation of quinoxaline rings. Also, the formation band broadening at 3500 cm^{-1} proves hydrogen bond network formation. Therefore, tertiary amines of quinoxaline rings can react with the electron poor methylene of the epoxide ring and chemical bonding between $mSiO_2$ nanoparticles and PCQAs has probably occurred. The reaction of epoxide groups on the surface of $mSiO_2$ particles and tertiary amines of quinoxaline rings was also checked with DSC. The exothermic peak in the DSC curves in Figure 4(b) indicates that curing of epoxide groups with tertiary amines occurs in the temperature range of 70–80°C. Therefore, tertiary amines of quinoxaline rings can react with the electron poor methylene of the epoxide ring and chemical bonding between $mSiO_2$ nanoparticles and PCQAs has probably occurred. XRD measurements were conducted to examine the nature of the nanocomposites with respect to neat PCQAs. According to the results, PCQA7 and $mSiO_2$ are totally amorphous in nature which do not show any sharp diffraction peaks. The AFM images in Figure 5 illustrates the surface morphology of pure PCQA1 (a) and its nanocomposites (15 wt % $mSiO_2$ (b) and 30 wt % $mSiO_2$ (c). It can be seen that the surface roughness is very small for the case of neat PCQA while the surfaces of nanocomposites containing SiO_2 are somewhat rough. SEM images of the top view and fractured surface of nanocomposite films of PCQA5/30 wt % $mSiO_2$ in Figure 6(a,b), respectively, show the uniform dispersion of nanoparticles in the polymer matrix (can be seen as white spots) and the roughness of the fracture surface indicating the improved toughness. Also TEM image of the hybrid film in Figure 6(c) shows dispersion of $mSiO_2$ particles in the polymer matrix.

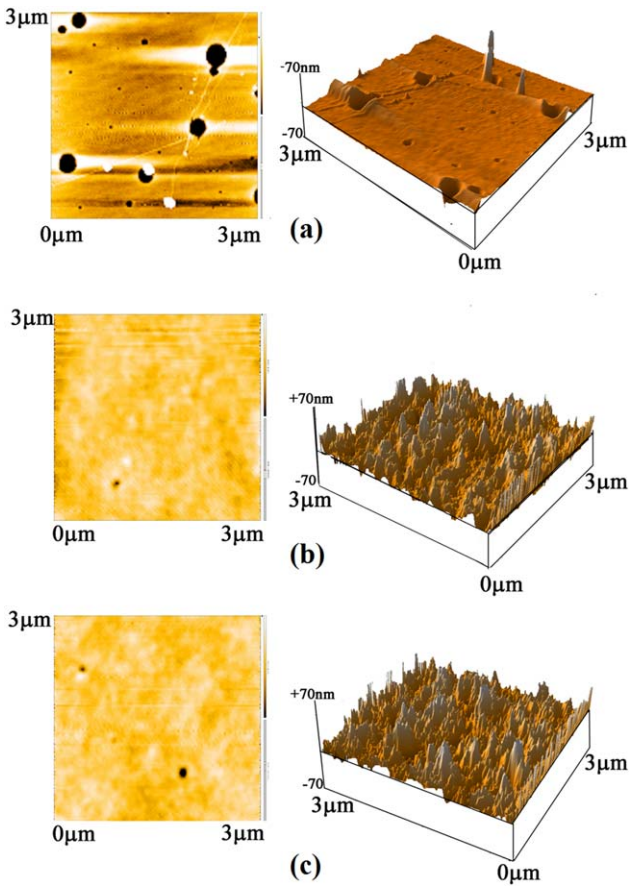

Figure 5. AFM images of (a) pure PCQA1, (b) PCQA1/15% $mSiO_2$, and (c) PCQA1/30% $mSiO_2$. [Color figure can be viewed in the online issue, which is available at wileyonlinelibrary.com.]

Solubility of PCQAs and Nanocomposites

The solubility of PCQAs and nanocomposites were investigated qualitatively and the results are listed in Table I. The solubility behavior of polymers depends on their chain packing abilities and intermolecular interactions, which in turn are influenced by the rigidity, symmetry, and regularity of the polymer backbone. Almost all PCQAs exhibited excellent solubility in strong aprotic solvents such as NMP, DMSO, DMAc, or DMF and even in less-polar solvents like pyridine in room temperature. Thus, these polymers can be solution cast into polymer films easily. The excellent solubility of these polymers can be attributed to presence of heterocylic rings and long flexible alkyl chain in the polymer backbone which disturb the planarity of aromatic units, reduce the close packing and crystallinity; and consequently, the solvent molecules were able to penetrate more easily to solubilize the polymer chains. PCQA5, PCQA6, and PCQA7 exhibited better solubility in aprotic solvents in comparison with aromatic polyamides PCQA1–3 and complete solubility in protic solvent of *m*-cresol at room temperature. This can be due to presence of aliphatic chain in the backbone of PCQA6 and PCQA7 and as side chains in both structural units of PCQA5. Comparison of the solubility of the previously reported polyamides with these polymers indicate that presence of long alkyl side chain and phenyl side group in the backbones

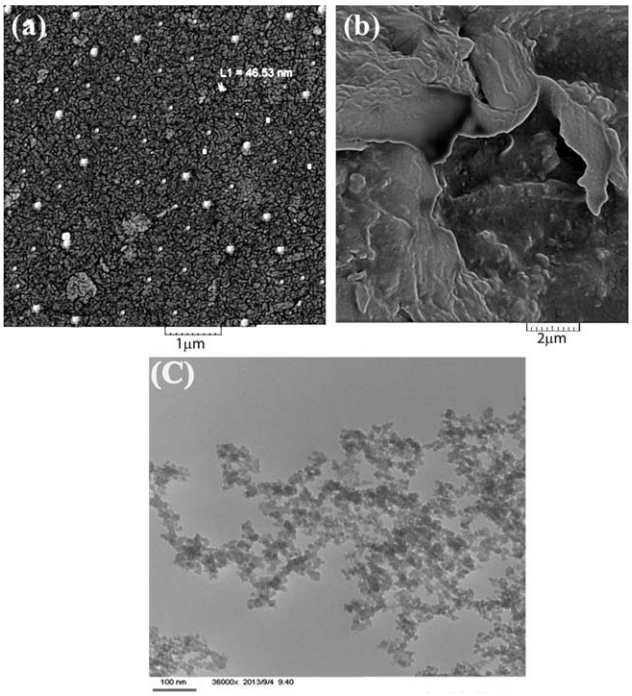

Figure 6. (a) SEM image of top view of PCAQ5/30% $mSiO_2$film, (b) SEM image of fracture surface of PCAQ5/30% $mSiO_2$ film, and (c) TEM image of PCAQ5/30% $mSiO_2$ film.

of theses polymers can improve the solubility in spite of presence of rigid units such as quinoxaline and carbazole rings in the main chains.[33,34] Nanocomposite films of PCQAs with 15 wt % of $mSiO_2$ did not dissolve in highly polar solvents such as NMP, DMF, DMSO, and DMAc at room temperature but showed limited solubility in at 60°C, and samples containing 30 wt % $mSiO_2$ did not dissolve on heating. These results reveal that nanocomposites prepared from $mSiO_2$ have definitely formed cross-linked network structure through chemical bonding between epoxide rings in the $mSiO_2$ and tertiary amines of heterocyclic rings and amide linkages.

Thermal and Mechanical Properties of PCQAs and Nanocomposites

The thermal behavior of PCQAs and their composites was evaluated by DSC, DMTA, and TGA. Neither crystallization exotherms nor melting endotherms were observed by DSC curves, as shown in Figure 4(b), in the range of 30–350°C, so that these polymers were considered to be essentially amorphous. Most of the general aromatic polyamides including the *p*-terphenylene polyamides are highly crystalline, since they do not have any side groups.[35] The fact that all PCQAs are amorphous can be ascribed to the effect of the incorporation of phenyl rings and long alkyl side chain, which must interrupt the intermolecular hydrogen bonding of the amide groups and disturbs the coplanarity of aromatic rigid units, and this reduces the interchain packing efficiency. Quenching from an elevated temperature of about 350°C to room temperature gave predominantly amorphous samples so that the T_g values of all PCQAs could be easily revealed in the subsequent DSC scans. The results are summarized in Table II. The T_g values PCQAs were measured in the range of 187–321°C by DSC, which followed the decreasing order of the chain flexibility and steric hindrance of the polymer backbones. In general, incorporation of less symmetric m-phenylene unit in PCQA2 and PCQA3 (307°C and 315°C, respectively) in comparison with PCQA1 (321°C) containing para-substituted ring or introduction of flexible aliphatic structure in the backbone of PCQA6 and PCQA7 (195°C and 187°C, respectively) have led to a decrease in T_g values. PCQA5 which was prepared from DAQC and CAQA has also showed lower T_g value (232°C) in comparison with the aromatic PCQAs. This

Table II. Thermal and Mechanical Properties of PCQAs and Nanocomposites

	Thermal properties					Mechanical properties		
Polymer Code	T_g(°C)[a]	T_g (°C)	T_5 (°C)[a]	T_{10} (°C)	Char yield (%)[b]	Tensile strength (MPa), (SDT)[c]	Elongation at break (%), (SDT)	Young's modulus (MPa), (STD)
PCAQ 1	-	321	432	478	67	-	-	
PCAQ 2	-	307	418	476	62	-	-	
PCAQ 3	-	315	408	458	60	-	-	
PCAQ 4	-	-	402	461	69	-	-	
PCAQ 5	235	232	390	463	60	100, (8.1)	11, (1.1)	3230, (34.8)
PCAQ 6	-	195	412	450	61	-	-	
PCAQ 7	200	187	408	445	57	90, (6.0)	13, (1.5)	2240, (22.2)
PCAQ5/ 15%$mSiO_2$	262	240	425	490	78	139, (11.7)	9, (1.3)	6060, (40.8)
PCAQ5/ 30%$mSiO_2$	270	255	436	500	82	150, (10.2)	4.5, (0.36)	9265, (59.6)

[a],Glass transition temperature was recorded by DMTA and DSC, respectively, at 10 °C/min in N_2.
[b],Temperatures of 5% and 10% weight loss, respectively, was recorded by TGA at 10 °C/min in N_2.
[c]Percentage weight of material left in TGA test at 600 °C in N_2.
[d]Standard deviation of five measurement.

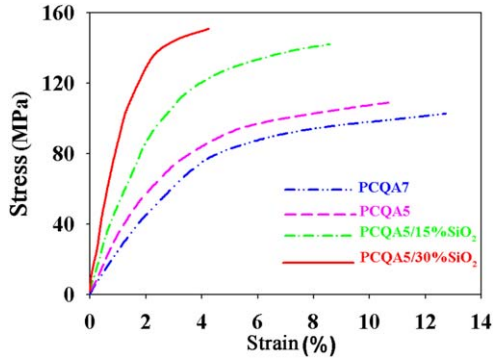

Figure 7. Tensile stress vs. strain (%) curves of representative PCQAs and nanocomposites. [Color figure can be viewed in the online issue, which is available at wileyonlinelibrary.com.]

can be due to bulky structure of the repeating units of this polymer as a result of the presence of more phenyl rings and long aliphatic side chains which increase the free volume and decrease the interchain interactions.

The viscoelastic behavior of the representative PCQA and nanocomposite was investigated by DMTA. Measurements of tan δ values, as shown in Figure 4(c), were carried out to relate the viscoelastic behavior of the polymer with $mSiO_2$ content in the composites. The T_g values of the representative PCQA5 and PCQA7 from the tan δ peak are 235°C and 200°C which are close to the values measured by DSC. It can be observed in Figure 4(c) that in the presence of $mSiO_2$ particles the value of tan δ drops and the peak shifted toward higher temperatures. This indicates that a change in the viscoelastic behavior of the nanocomposite films from liquid like to solid-like occurs. Figure 4(d) shows thermoplastic response by plotting storage modulus values as a function of varying wt % of SiO_2 particles against testing temperature. It is observed that with increasing SiO_2 nanoparticles content the value of storage modulus increases. These changes can reveal the occurrence of reactions of cross-links formation between $mSiO_2$ particles and polyamide chains during solution blending. These reactions immobilize the polymer chains at elevated temperature. The β-relaxation processes were observed from around 100°C for PCQA/15 wt % $mSiO_2$ and appeared below 50°C for PCQA/30 wt % $mSiO_2$ which can be due to local molecular motions related to the flexible aliphatic chain of the GPTES modifier. The thermal stability was evaluated by TGA in N_2 and the typical curves of representative PCQA are shown in Figure 4(a). The temperatures of 5% and 10% weight loss (T_5 and T_{10}) and the char yields at 600°C are listed in Table II. All these polyamides exhibited good thermal stability up to 400°C and began to lose weight gradually above this temperature. The T_{10} value of these polyamides stayed within 445–478°C and they left more than 57% char yield. PCQA1 containing *p*-substituted phenylene ring in the backbones has the highest ($T_{10} = 478$°C) and the semialiphatic PCQA7 has the lowest ($T_{10} = 445$°C) thermal stability. The experimental results indicated that these polyamides possessed great thermal stability due to presence of quinoxaline and carbazole rings in the main chains and are able to withstand the harsh environments of many high-tech applications such as

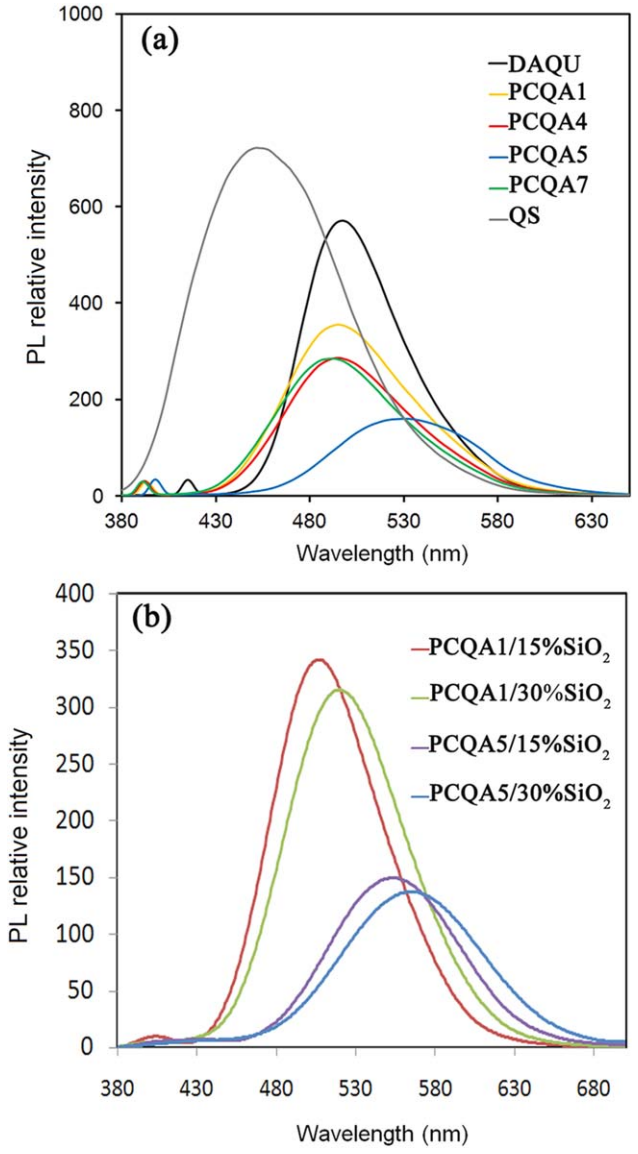

Figure 8. Fluorescence spectra of (a) Some PCQAs in NMP solution and (b) Some PCQAs nanocomposite thin films. [Color figure can be viewed in the online issue, which is available at wileyonlinelibrary.com.]

microelectronic manufacturing and packaging industry. TGA curves in Figure 4(a) show that the weight loss of native SiO_2 is 0.5% at the range of 0–400°C (almost no weight loss over 400°C); it is mainly due to the loss of absorbed moisture. The weight of $mSiO_2$ decreases quickly over 300°C and the loss is about 25% over 500°C, which can be attributed to the thermal decomposition of GPTES at high temperature. Therefore, the maximum mass fraction of GPTES on the surface of SiO_2 is ~25%. The existence of inorganic materials in polymer matrix, generally, enhances the thermal stability of the composite. In the present case also, the thermal stability is expected to increase due to the presence of the inorganic phase and its interaction with the polymer. The nanocomposite of PCQA5 containing 15 wt % $mSiO_2$ particles showed high thermal stability (T_{10} has increased from 463°C to 490°C). However, as can be seen in Figure 4(a) and Table II, increasing the amount of

Table III. Optical Properties of PCQAs and Nanocomposites

	In solution			As film	
Polymer code	abs λ_{max}(nm)[a]	PL λ_{max}(nm)[a]	Φ_F(%)[a]	abs λ_{max}(nm)	PL λ_{max}(nm)
PCQA1	395	496	44.72	414	509
PCQA 2	395	496	37.10	414	508
PCQA 3	395	500	23.75	412	515
PCQA 4	393	495	41.22	409	509
PCQA 5	400	530	12.79	417	548
PCQA 6	392	494	34.40	407	508
PCQA 7	392	490	36.31	407	504
PCQA1/15%SiO_2	-	-	-	425	515
PCQA1/30%SiO_2	-	-	-	438	525
PCQA5/15%SiO_2	-	-	-	425	560
PCQA5/15%SiO_2	-	-	-	439	570

[a] Measured in dilute solution in NMP at a concentration of about 0.02 g/dL.
[b] The quantum yield in dilute solution was calculated in an integrating sphere with quinine sulfate as the standard ($\Phi_{F=}$ 54.6%).

$mSiO_2$ from 15 wt % to 30 wt % did not increase thermal stability of polymer much, T_{10} increased only 10°C. This can be due to modification of inorganic SiO_2 particles with the organic silane modifier. In fact, increasing the amount of $mSiO_2$ particles increases the amount of organic phase of the composite which has lower thermal stability than inorganic phase. The mechanical properties of PCQAs and the nanocomposites were measured in the tensile mode and the typical stress–strain curves are illustrated in Figure 7. As can be seen in this figure, PCQA7 showed lower strength and higher elongation due to presence of aliphatic chain in the backbone and also lower molecular weights in comparison with the PCQA5. The tensile strength and the modulus of PCQAs increased with the addition of SiO_2 nanoparticles up to 30 wt %; and simultaneously, the tensile elongation decreased. The tensile strength has increased from 90 MPa for the neat PCQA7 to 100 MPa and 139 MPa and 150 MPa for PCQA5, PCQA5/15% SiO_2, and PCQA5/30% SiO_2, respectively, and also elongation at break decreased from 13 to 11, 9 and 4.5%. These effects can be mainly attributed to the strong interactions between SiO_2 and PCQAs matrix via formation of covalent bonds. Therefore, network formation strengthens the material and increase the modulus while reduce the flexibility and decrease elongation. Also, the fine dispersion and a certain extent of orientation of SiO_2 in PCQAs matrix can lead to the efficient load transfer from the PCQAs matrix to SiO_2 nanoparticles and less stress convergence during the elongation process.

Photophysical Properties of PCQAs and Nanocomposites

The photophysical properties of the prepared polyamides and nanocomposites were investigated by UV–vis and photoluminescence (PL) spectroscopy. The UV–vis and photoluminescence data are summarized in Table III. The maximum absorption wavelengths (λ_{ab}) of PCQAs in dilute NMP solutions (0.02 g dL^{-1}) were at 392–400 nm and in solid state at 407–417 nm which can be attributed to the electronic transitions (π–π^*) of long conjugation along the polymers backbones, and the highest λ_{ab} values belong to PCQA5 which contains more chromophore units in its repeating unit.

The PL emission spectra of dilute NMP solutions of diamine (DAQC) (10^{-5} *M*) and PCQAs (0.02 g dL^{-1}) are shown in Figure 8(a). The emission spectrum of each polyamide was recorded with excitation at its maximum absorption wavelength. DAQC showed strong blue fluorescent light with the maximum emission wavelength at $\lambda_{em} = 490$ nm. The λ_{em} of PCQAs in solution were observed in the region of 490–530 nm and for the films were red-shifted relative to solution and observed at 504–548 nm. The fluorescence quantum yields (Φ_f) of PCQAs in NMP solutions were measured relative to quinine sulfate (QS) with $\lambda_{em} = 450$ nm and $\Phi_f = 0.54$. PCQAs showed moderate Φ_f values ranged from 22% to 41%, as listed Table III.

The red-shifted emission maxima and the narrow band gap of the films relative to that of solutions suggest the tendency of polymers to create aggregates in solid state. It is obvious that in solid state both intra and inter chain interactions play important role on photophysical properties of the polymers. The PL emission spectra of films of PCQA1/15 wt % $mSiO_2$, PCQA1/30 wt % $mSiO_2$, PCQA5/15 wt % $mSiO_2$, and PCQA5/30 wt % $mSiO_2$ nanocomposites are shown in Figure 8(b), and their important optical data are listed in Table III. The absorption peak and also the fluorescence emission peak of the nanocomposites films were red-shifted with the addition of $mSiO_2$ and showed dependence on the amount of nanoparticles.

Water Absorption and Removal of Metal Ions From Aqueous Solution by PCQA5 and Nanocomposites

Polyamides are hydrophilic polymers due to their polar amide groups, whose interaction with water leads to a water uptake from the environment. The polyamides described in this work have two amide groups and two substituted aromatic moieties per structural unit. In general, the loose packing of polymer chains due to bulky pendant results in the increase in free

volume that should ensure the polymer to entrap some of the water molecules. Two methods, according to literature were used for the water absorption measurement of PCQAs.[36] Water absorption of the polymer films were in the range of 5–9.2% and 7.2–11.6% at room temperature and at 100°C, respectively. On the other hand, PCQA4 exhibited the lowest water absorption due to the hydrophobic nature of the trifluoromethyl groups and PCQA5 showed the highest water absorption as a result of many hydrophilic groups in its repeating unit.

Toxic metal ions can be found in a variety of natural sites, such as river water or lake water, as well as in biological and inorganic–organic samples. The necessity to reduce metal ion concentrations to acceptable levels in wastewater and the need for more highly specific metal ion-recovery processes have led to increasing interest to develop new technologies. As the synthesized polymers are insoluble in water, therefore, solid–liquid extractions have been carried out with PCQA5 because of its high water uptake. Extraction of metal ions such as Cr^{3+}, Co^{2+}, and Cd^{2+} as their chloride salts, Hg^{2+} and Pb^{2+} as nitrate salt and Cr^{6+} as $Cr_2O_7^{2-}$ was carried out from aqueous solutions either individually or in the mixture. In these experiments, the quinoxaline heterocyclic and the amide linkages of the solid polymer acted as hosts for the target metal ion and the metal ions embed in the polymer matrix by physical Interaction. The amount of adsorbed ions was calculated using the following equation:

$$Q_t = (C_0 - C_A) \times V / W \quad (1)$$

where Q_t is the amount of metal ions adsorbed into the unit of the composites (mg g^{-1}), C_0 and C_A are the concentrations of metal ions in the initial solution and in the aqueous phase after adsorption, respectively (mg mL^{-1}), V is the volume of the aqueous phase (mL), and W is the weight of the polymer (g). The efficiency for ions adsorption from the solution (%R) was calculated using the following:

$$R = (C_i - C_e)/C_i \times 100 \quad (2)$$

where C_i and C_e are the initial and at the equilibrium concentration of ion in solution, respectively. Figure 9(a) depicts the solid–liquid extraction results for the elimination of individual metal cations from aqueous solution of pH = 8 at 25°C. As can be seen in this figure, both parameters Q_t and %R increased in order of $Co^{2+} > Cr^{3+} > Cd^{2+} > Hg^{2+} > Pb^{2+} > Cr^{6+}$ which is opposite of the order of their ionic radius. This can probably suggest the amide and quinoxaline groups present in the polymer backbone are responsible for the higher efficiency toward the adsorption metal ions from aqueous solutions and free space between the polymer chains can allocate a place for the metal ions. The effect of pH on Co^{2+} extraction of PCQA5 is given in Figure 9(b). The pH values were varied between 1.0 and 14.0. In adsorption studies, pH is a critical parameter because it influences the chemistry of active binding sites on the adsorbent.

As can be seen in Figure 9(b), extraction of Co^{2+} ion is low in the acidic region (pH = 1–5), then starts to increase with increasing pH and takes its maximum value in the basic region

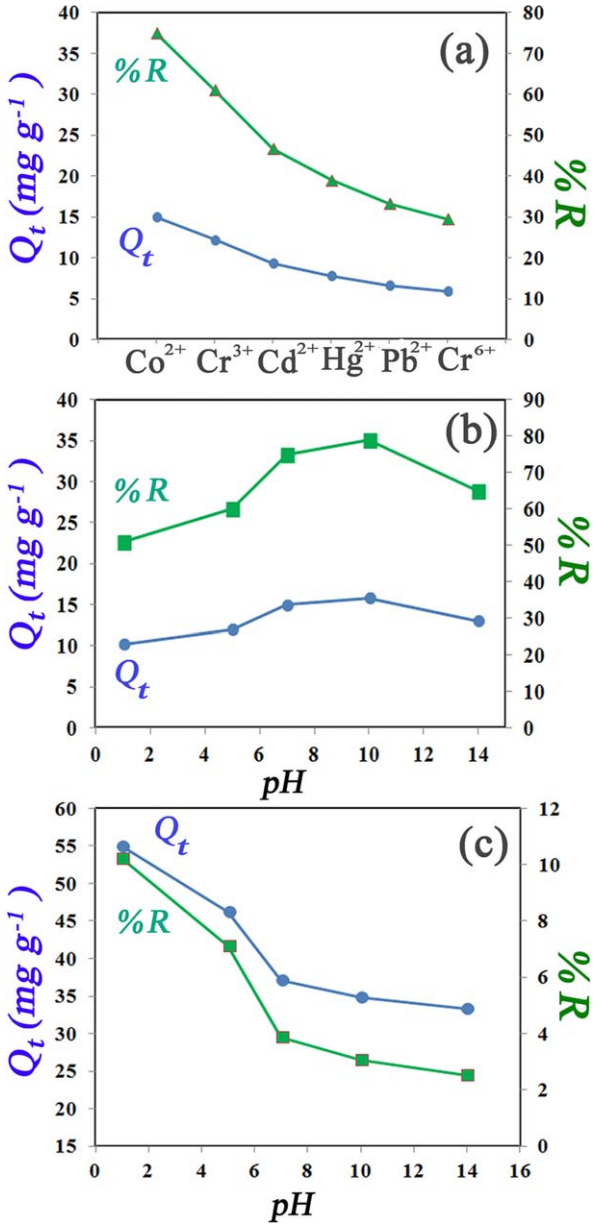

Figure 9. Metal cations adsorption capacity (Q_t) and efficiency (%R) by PCQA5 (a), effect of variation in pH on the adsorption quantity of Co^{2+} (b) and Cr^{6+} as $Cr_2O_7^{2-}$ (c) by PCQA5. [Color figure can be viewed in the online issue, which is available at wileyonlinelibrary.com.]

of pH about 10.0. This result indicates that protonation of more basic pyridine-type nitrogen in the quinoxaline rings in acidic condition reduced capability of polymer for metal ion extraction, and the decrease in extraction of metal ion at pH 14 can be due to high concentration of hydroxyl ions (OH^-) in the solution which compete with the polymer chain in metal ion absorption. Figure 9(c) shows the extraction efficiency of $Cr_2O_7^{2-}$ by the polymer depends of the acidity of the extraction condition (pH). The pyridine-type nitrogen is protonated at low pH (i.e., pH 1.0–2.0) and the negatively charged chromate ions become electrostatically attracted to the positively charged amine groups of the polymer chains. Selectivity coefficient of adsorption of metal ions in the solution

Table IV. Distribution Coefficient (K_d) and Selectivity (α) in Competitive Conditions

	Distribution coefficient (K_d, ml g^{-1})			Selectivity factor (α)		
Ion	PCQA5	PCQA5/15%SiO_2	PCQA5/30%SiO_2	PCQA5	PCQA5/15%SiO_2	PCQA5/30%SiO_2
Cr^{VI}	333	449	680	0.12	0.11	0.07
Pb^{II}	452	538	870	0.15	0.13	0.09
Hg^{II}	600	666	1127	0.21	0.16	0.12
Cd^{II}	834	1222	1531	0.30	0.30	0.17
Cr^{III}	1500	2333	4555	0.54	0.58	0.50
Co^{II}	2752	4000	9000	1	1	1

was studied in the mixture by batch procedure.[37] The distribution coefficients (K_d) of ions were determined by the following equation:

$$K_d = [(C_0 - C_A)] \times V / C_A \times W \quad (3)$$

$$\alpha = K_d M^{n+} / K_d Cr^{3+} \quad (4)$$

where V is the volume of initial solution and W is the mass of polymer, C_0 and C_A are initial and final concentrations of metal ions. The extraction selectivity, α, is the ratio of two distribution coefficients and calculated by in eq. (4). The ion Co^{2+} was taken as the reference, as it has the highest distribution coefficient. The results of selectivity in the mixture of metal cations in solution are shown in Table IV. As can be seen in this table, the selective extraction of ion Co^{2+} in the mixture solution of metal ions Hg^{2+}, Cr^{3+}, Pb^{2+}, and Cd^{2+} is the highest which is similar to the results obtained for each ion individually. It is clear from the selectivity factor that the quantitative separation of ion Co^{2+} from the rest of the ions is possible.

As can be seen in Table IV, the nanocomposites have higher efficiency of ions extraction in comparison with that of PCQA5, and the distribution coefficient increased with the content of nanosilica in the polymer matrix. The extraction level of these ions from aqueous media by these polymers present their future applications in the fields of water decontamination, membrane preparation for cation transport and in sensing materials, among other applications.

CONCLUSIONS

The objective of this work was two folds: (1) design and synthesis of new thermally stable, organosoluble and fluorescent aramides containing luminescent functional groups in the main chains and (2) preparation of reinforced and thermally stable nanocomposites with nanosilica by epoxide functionalization. Therefore, an aromatic diamine containing substituted carbazole and quinoxaline moieties was synthesized, characterized and used for preparation of aramids using different aromatic and aliphatic dicarboxylic acids. The obtained organosolubles aramids with $\overline{M}_w$ in the range of 51,630–58,470 g mol^{-1} exhibited good film-forming capability and reasonable thermal stability (T_g = 187–321°C and $T_{10\%}$ = 445–478°C) suitable for thermoforming processing. These results support that such a modification of the polymer structure can be used as an effective strategy for imparting fluorescence emission in the visible light region and enhancing the processability of aramids, while maintaining the high thermal stability. These polymers with active sites in the backbone were also used in the preparation of reinforced composite materials with the epoxide functionalized nanosilica. As compared with the pure PCQAs, the $mSiO_2$ nanoparticles have improved properties of nanocomposites such as thermal and tensile strength due to increased interfacial interaction between $mSiO_2$ and the polymer matrix while the elongation at break decreased. The results also demonstrated that these aramids and particularly their nanocomposites can act efficiently as chelating agent for heavy metal ions.

REFERENCES

1. Garcia, J. M.; Garcia, F. C.; Serna, F.; De la Pena, J. L. *Prog. Polym. Sci.* **2010**, *35*, 623.
2. Liaw, D. J.; Liaw, B. Y.; Yang, C. M.; Hsu, P. N.; Hwang, C. Y. *J. Polym. Sci. Part A: Polym. Chem.* **2001**, *39*, 1156.
3. Onciu, M. *J. Appl. Polym. Sci.* **2007**, *103*, 2013.
4. Hsiao, S. H.; Chen, C. W.; Liou, G. S. *J. Polym. Sci. Part A: Polym. Chem.* **2004**, *42*, 3302.
5. Pal, R. R.; Patil, P. S.; Salunkhe, M. M.; Maldar, N. N.; Wadgaonkar, P. P. *Eur. Polym. J.* **2009**, *45*, 953.
6. Ghaemy, M.; Amininasab, S. M.; Alizadeh, R. *J. Appl. Polym. Sci.* **2010**, *116*, 3725.
7. Liou, G. S.; Hsiao, S. H.; Haung, N. K.; Yang, Y. L. *Macromolecules* **2006**, *39*, 5337.
8. Ghaemy, M.; Alizadeh, R.; Behmadi, H. *Eur. Polym. J.* **2009**, *45*, 3108.
9. Ghaemy, M.; Barghamadi, M. *J. Appl. Polym. Sci.* **2009**, *114*, 3464.
10. San-José, N.; Gómez-Valdemoro, A.; García, F.; Serna, F.; García, J. *J. Polym. Sci. Part A: Polym. Chem.* **2007**, *45*, 4026.
11. Ghaemy, M.; Behmadi, H.; Alizadeh, R. *Chin. Chem. Lett.* **2009**, *20*, 961.
12. Liaw, D. J.; Hsu, P. N.; Liaw, B. Y. *J. Polym. Sci. Part A: Polym. Chem.* **2001**, *39*, 63.
13. Liu, Y. L.; Tsai, S. H. *Polymer* **2002**, *43*, 5757.
14. Liou, G. S.; Hsiao, S. H.; Ishida, M.; Kakimoto, M.; Imai, Y. *J. Polym. Sci. Part A: Polym. Chem.* **2002**, *40*, 2810.

15. Ghaemy, M.; Porazizollahy, R.; Bazzar, M. *Macromol. Res.* **2011**, *19*, 528.
16. Patil, V.; Sayyed, M.; Mahanwar, P.; Wadgaonkar, P.; Maldar, N. *J. Polym. Res.* **2011**, *18*, 549.
17. Shi, W.; Wang, L.; Zhen, H.; Zhu, D.; Awut, T.; Mi, H.; Nurulla, I. *Dyes Pigments* **2009**, 83.
18. Thlelakkat, M. M.; Posch, P.; Schmidt, H. W. *Macromolecules* **2001**, *34*, 7441.
19. Jonforsen, M.; Johansson, T.; Inganas, O.; Andersson, M. R. *Macromolecules* **2002**, *35*, 1638.
20. Moon, I. K.; Choi, C. S.; Kim, N. *Polymer* **2007**, *48*, 3461.
21. Grazulevicius, J. V.; Strohriegl, P.; Pielichowski, J.; Pielichowski, K. *Prog. Polym. Sci.* **2003**, *28*, 1297.
22. Natera, J.; Otero, L.; Sereno, L.; Fungo, F.; Wang, N. S.; Tsai, Y. M.; Hwu, T. Y.; Wong, K. T. *Macromolecules* **2007**, *40*, 4456.
23. Catauro, M.; Raucci, M. G.; Gaetano, F.; Buri, A.; Marotta, A.; Ambrosio. L. *J. Mater. Sci. Mater. Med.* **2004**, *15*, 991.
24. Tommalieh, M. J.; Zihlif, A. M. *Phsica B: Condensed Matter* **2010**, *405*, 4750.
25. Preghenella, M.; Pegoretti, A.; Migliaresi, C. *Polymer* **2005**, *46*, 12065.
26. Sengupta, R.; Bandyopadhyay, A.; Sabharwal, S.; Chaki, T. K.; Bhowmick, A. K. *Polymer* **2005**, *46*, 3343.
27. Bazzar, M.; Ghaemy, M.; Alizadeh, R. *Polym. Degrad. Stab.* **2012**, *97*, 1690.
28. Yamazaki, N.; Matsumoto, M.; Higashi, F. *J. Polym. Sci. Polym. Chem. Ed.* **1975**, *13*, 1373.
29. Ghaemy, M.; Hashemi Nasr, F.; Alizadeh, R.; Taghavi, M. *Macromol. Res.* **2012**, *20*, 614.
30. Ricciardi, F.; Romanchick, W. A.; Jouille, M. M. *J. Polym. Sci. Polym. Chem. Ed.* **1983**, *21*, 1475.
31. Ghaemy, M.; Sadjady, S. *J. Appl. Polym. Sci.* **2006**, *100*, 2634.
32. Ryu, B. Y.; Emrick, T. *Macromolecules* **2011**, *44*, 5693.
33. Chao, C. S.; Whang, W. T.; Hung, C. H. *Macromol. Chem. Phys.* **2001**, *202*, 2864.
34. Zhang, Y.; Wada, T.; Sasabe, H. *J. Polym. Sci. Part A: Polym. Chem.* **1996**, *34*, 2289.
35. Li, Z. B.; Ueda, M. *J. Polym. Sci. Polym. Chem. Ed.* **1984**, *22*, 3063.
36. Xie, K.; Zhang, S. Y.; Liu, J. G.; He, M. H.; Yang, S. Y. *J. Polym. Sci. Part A: Polym. Chem.* **2001**, *39*, 2581.
37. Brown, P. A.; Gill, S. A.; Allen, S. J. *Water Res.* **2000**, *34*, 3907.